Control of Vortex Breakdown in a Closed Cylinder with a Small Rotating Rod

David LO JACONO[1], Jens N. SORENSEN[2], Mark C. THOMPSON[1,3] and Kerry HOURIGAN[1,3]

[1] *Fluids Laboratory for Aeronautical and Industrial Research (FLAIR), Department of Mechanical Engineering, Monash University, Melbourne, Australia*

[2] *Department of Mechanical Engineering, Technical University of Denmark, Copenhagen, Denmark*

[3] *Division of Biological Engineering, Monash University, Melbourne, Australia*

Abstract. Effective control of a vortex breakdown was achieved with small rotating rods. This study was performed experimentally and numerically with high precision. After validation with accurate measurements using a novel SPIV technique, analysis of numerical simulations has been undertaken. The effect of a finite partial rod creates additional source terms in the vorticity as it rotates. These additional source terms and their spatial location influence the occurrence of the vortex breakdown.

Key words: instability, transition, DNS, bluff-bodies, incompressible flow.

1. Introduction

The flow within a closed cylinder with a rotating lid is considered. This type of flow has been the focus of earlier studies involving vortex breakdown including relevance to bioreactor design (see for example [11, 2, 5, 7, 8, 1]). However, vortex breakdown is not fully understood and remains difficult to predict and control. Recently, there have been attempts to control this phenomenon. Hussain *et al.* [4] studied the addition of a rotating axial rod, and Herrada and Shtern [3]) investigated the introduction of temperature gradients. Mununga *et al.* [6]) studied the effect of a small rotating disk opposite to the driving lid. In this study, we propose to seek the effect on the vortex breakdown by a small rotating rod positioned along the centre axis. This will complete the knowledge of the two limiting cases studied previously. Experimental results undertaken in the cylindrical cavity will be presented for the axial rotating rod and for the partial rotating rod for several rotating configurations. In addition to these experiments, high order numerical simulations have been performed in order to provide additional accuracy.

2. Experimental setup

The experimental setup consists of a cylinder of diameter $D = 2R = 65$ mm that was filled with water and placed in the center of an octagonal shaped container, see Fig. 1. The octagonal shape allows the exterior faces of the rig to be flat in order to reduce refraction effects that result in optical distortion errors during the use of image-based measurement techniques. A flat, circular disk acted as the rotating bottom, and was located in the center of the base. The rod diameter used here was fixed to be $d = 3$ mm, and acted as the control device. For the partial rod

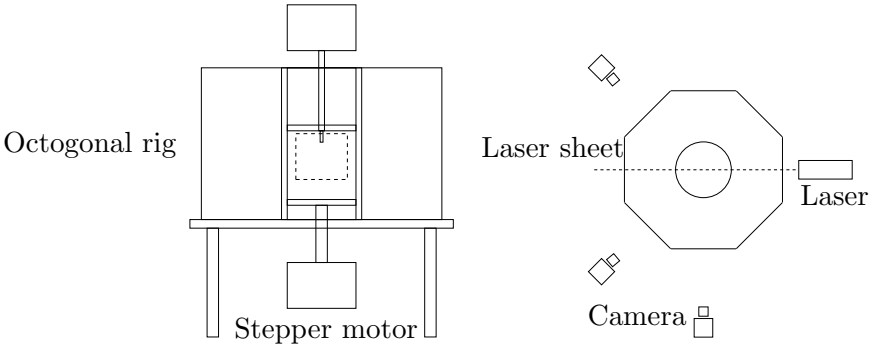

Figure 1. Experimental apparatus, here shown with a partial axial rod. Left: vertical cross-section, where the dotted window represents the SPIV-field. Right: Top view and SPIV setup.

experiments, an $l = 13$ mm height rod was used ($\lambda = l/R = 0.4$). The shafts of the disk and the rod were rotated by two independent small stepper motors via a high-performance motion controller. Stereoscopic Particle Image Velocimetry, SPIV, was the primary tool used for quantitative flow measurement. An angular displacement system was chosen, meaning that the two CCD cameras (PCO Imaging Pixelfly) were positioned at a fixed angle off center. Calibration was conducted using the third camera located normal to the laser sheet. The tracer particles used were silver coated hollow glass micro-spheres with a nominal diameter of 12 μm and were illuminated by a 1.0 mm thick light sheet powered by the 532 nm laser.

3. Computational method

The incompressible Navier-Stokes equations were solved using a spectral-element technique. The simulations were undertaken on a 400 macro-element mesh carefully distributed on the boundaries. The geometry was split into quadrilateral elements, and within these elements, the velocity and pressure fields were represented by seventh-order tensor-product polynomials, associated with Gauss-Lobatto-Legendre quadrature points. Details of this approach and implementation can be found in Thompson *et al.* [10]. Axisymmetry and no-slip boundary condition were applied on the appropriate sides of the computational domain.

4. Results and Discussion

The parameters governing the flow consist of the aspect ratio of the rig $H/R = 1.85$ which is kept constant, the Reynolds number $\mathrm{Re} = \omega_{\mathrm{lid}} R^2/\nu$, where ω_{lid} is the angular speed of the driving lid and ν is the kinematic viscosity, and the ratio between the two Reynolds number $\gamma = (\omega_{\mathrm{rod}} r^2)/(\omega_{\mathrm{lid}} R^2)$. All variables have been made dimensionless using R and ω_{lid} as reference length and velocity scales. All experimental data are non-dimensionalised with the previously defined characteristic scales to allow direct comparison with numerical results. The Reynolds number is kept constant and equal to 2200, and our main parameter will be γ.
Figures 2 and 3 show the effect of a thin rod for co-rotation and counter-rotation, respectively. These figures represent iso-contours of the axial velocity, and of interest is the zero value contour (solid line) delimiting the vortex breakdown. The additional

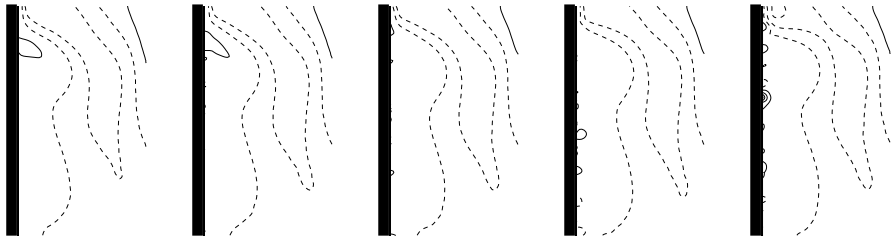

Figure 2. Effect of a co-rotating thin rod Re = 2200. Only the axial velocity is shown for several rotational speeds. Solid and dashed lines represent zero and negative axial velocities, respectively.

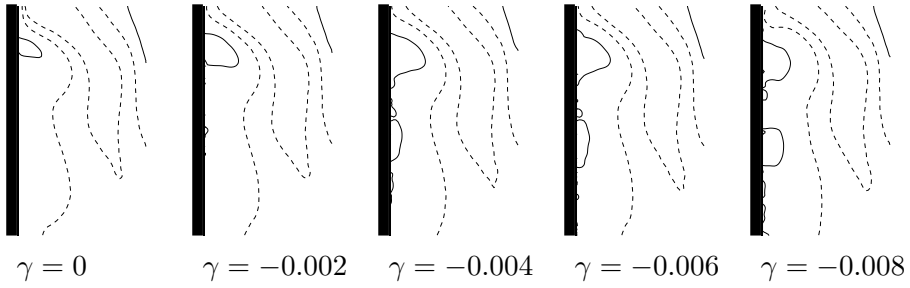

Figure 3. Effect of a counter-rotating thin rod Re = 2200. Only the axial velocity is shown for several rotational speeds. Solid and dashed lines represent zero and negative axial velocities, respectively.

swirl provided by the axial rod on the vortex breakdown is striking. For co-rotation, ($\gamma > 0$), the vortex breakdown diminishes and even vanishes with increasing γ. However, for counter-rotation, the effect is the opposite; the vortex breakdown increases in size and a second breakdown appears for decreasing γ. This variation of vortex breakdown with γ is qualitatively consistent with previous published work [4].

This introduction of a rotating rod will generate additional axial vorticity near the lid. The azimuthal vorticity component equation can be written in cylindrical coordinates (r, θ, z) as follows:

$$\frac{\partial \omega}{\partial t} = -\frac{\partial}{\partial r}(u_r \omega) - \frac{\partial}{\partial z}(u_z \omega) + \frac{1}{r}\frac{\partial}{\partial z}(u_\theta^2) + \frac{1}{\mathrm{Re}}\left[\frac{\partial}{\partial r}\left(\frac{1}{r}\frac{\partial r\omega}{\partial r}\right) + \frac{\partial^2 \omega}{\partial z^2}\right], \tag{1}$$

where the vorticity is $\omega = (\boldsymbol{\nabla} \times \boldsymbol{u}) \cdot \boldsymbol{e}_\theta$, the flow velocity $\boldsymbol{u} = (u_r, u_\theta, u_z)$ and $\boldsymbol{e}_\theta$ is the azimuthal unit vector. For a rod running throughout the cylinder, one significant way the rotational motion introduced by the rod can affect the vorticity, influencing in turn the flow behaviour in the meridional plane, is through the source term:

$$S = \frac{1}{r}\frac{\partial u_\theta^2}{\partial z} \tag{2}$$

At the curved surface of the rotating rod, the source term is null (u_θ does not vary with z). Away from the rod, the source term is expected not to have a significant

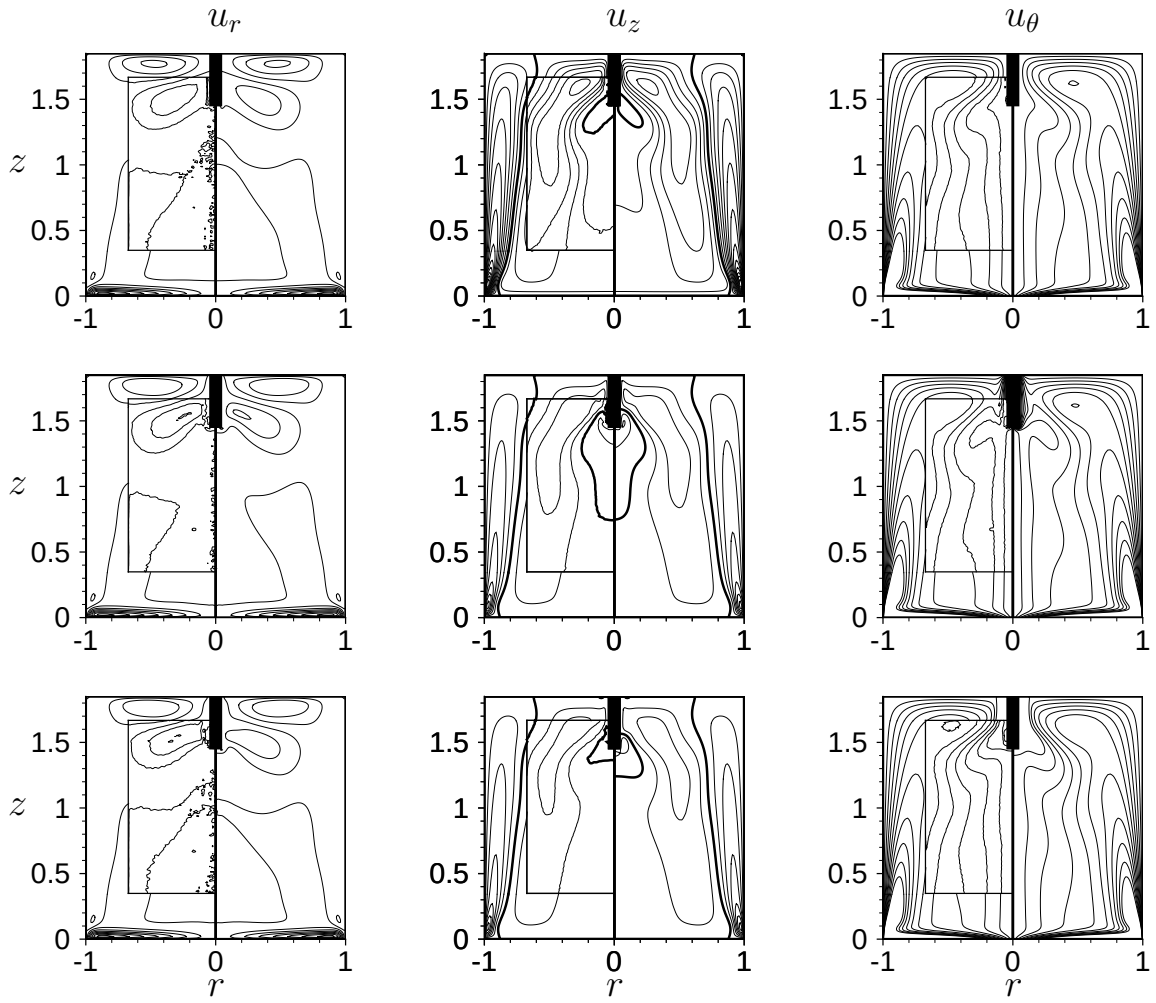

Figure 4. Comparison of velocity iso-contours of the SPIV results at Re = 2200 and $H/R = 1.85$, with numerical simulations, for a thin partial rod ($\lambda = 0.4$). Top row: the rod is not rotating, $\gamma = 0.0$. Middle row: the rod rotation is set to $\gamma = 0.1$. Bottom row: the rod rotation is set to $\gamma = -0.1$. The experimental iso-contours region are shown in the window at the left hand side of each image and are surrounded by the numerical iso-contours.

effect on the flow as the azimuthal velocity introduced by the rotating rod is mainly a function of r. However, close to the rod and especially near the lid, the azimuthal velocity experiences a jump from the constant rotating speed of the rod and the surrounding flow. This source term will generate a velocity field according to the Biot–Savart induction law.

In order to investigate the physics underlying the mechanism, additional experiments have been undertaken. The full axial rod used by Hussain *et al.* [4] has been replaced with the partial thin axial rod ($\lambda = 0.4$). It was verified that the introduction of a small *non-rotating* rod has no significant effect on the flow into which it is introduced. In these types of flow, it has been found that even the slightest imperfections in the apparatus will create asymmetries [9]. In order to validate against an axisymmetric CFD simulation, flow measurements have been averaged over the two half planes to produce symmetric data.

Figures 4 shows the comparison of matched iso-contours for the velocity components

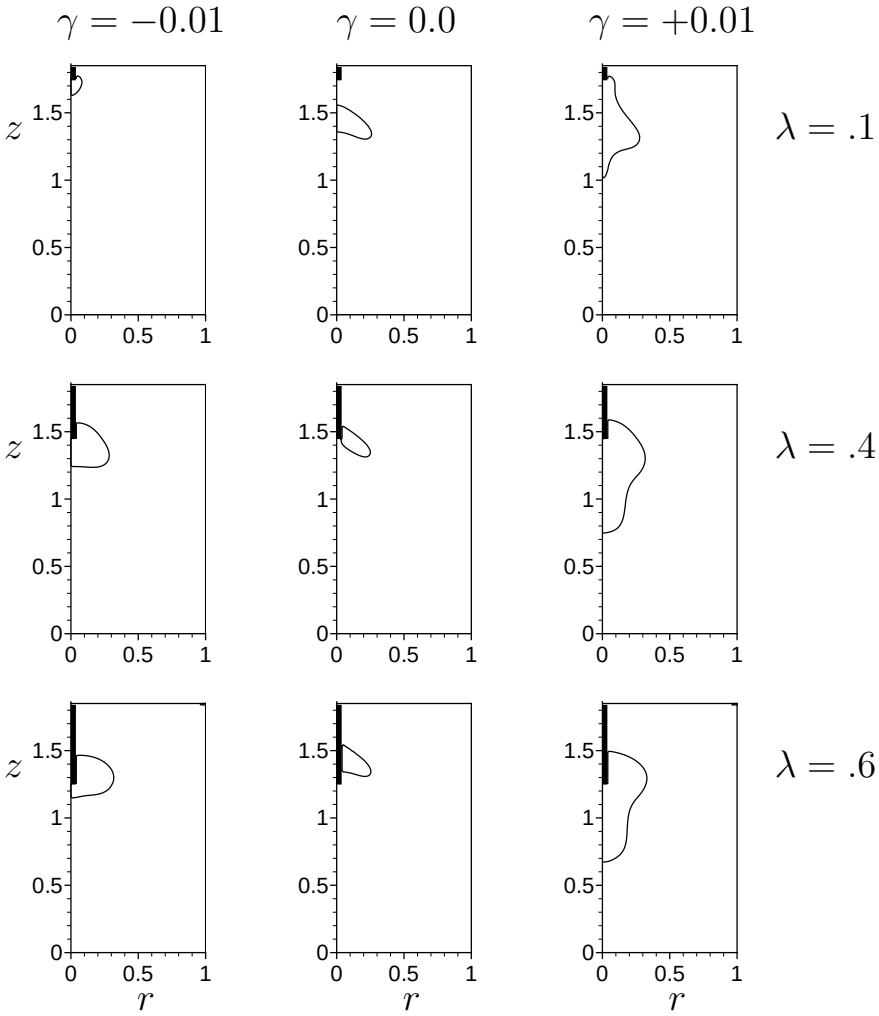

Figure 5. Numerical simulations performed for several rod lengths. The iso-contour represented is the zero-streamline, in other words the boundary of the recirculation zone. Clearly if the length, λ, approaches zero, the recirculation zone is more likely to vanish. Interestingly, the pattern for the longer rods ($\lambda = 0.4$ and $\lambda = 0.6$) change little.

between symmetric experimental data (in the boxed region) and numerical data (in the surrounding region) for the non-rotating ($\gamma = 0.0$), co-rotating ($\gamma = 0.01$) and counter-rotating ($\gamma = -0.01$) small rod cases, respectively. Note the excellent agreement between the numerical and the experimental data. It should be recalled that there is no smoothing or filtering of the experimental data from the SPIV process.

By inserting a small rotating rod, the recirculation region has been modified. But unlike for the full axial rod, co- or counter-rotating the short rod does not affect the bubble in the same fashion. This may be due by two different reasons: first, near the rotating lid and the long thin rod (at $z = 0$), there was a source term which does not appear with a short rod; second, near the edge of the small rod (at $z \approx 1.45$), a source term coming from the radial velocity ejected at the edge of the rotating rod appears. This complicates the physical phenomena occurring with the recirculation bubble. Further investigation with numerical simulation has been undertaken for various length of rods.

Figure 5 shows the results of varying the lengths of the rod on the recirculation zone. As the rod shortens and approaches the shape of a flat disk on the upper lid ($\lambda \to 0$), the recirculation zone disappears for counter-rotation. This result is similar to that of Mununga *et al.* [6], where a disk flush with the upper-lid is rotating. Further studies to elucidate the action of a *finite*-length rod are currently under process.

5. Conclusions

The effect of a finite width full and short rod on the vortex breakdown in a confined cylindrical cavity has been investigated by means of experiments and numerical simulation. The measured experimental velocity field and numerical simulation are in a good agreement. For a long axial rod, it was confirmed that the co-rotation suppresses the vortex breakdown, unlike counter-rotation which enhances the vortex breakdown region. For short rod length, additional vorticity source terms complicate the behaviour of the recirculation zone when the rod rotates. As the rod shortens, the breakdown behaviour approaches the limit of a flat disk and the recirculation bubble vanishes for sufficient counter-rotational speed.

Acknowledgements

DL thanks the Swiss National Science Foundation for their support.

References

[1] J. Dusting, J. Sheridan, and K. Hourigan. A fluid dynamics approach to bioreactor design for cell and tissue culture. *Biotechnology and Bioengineering*, 94(6), 2006.

[2] M.P. Escudier. Observations of the flow produced in a cylindrical container by a rotating endwall. *Exp. Fluids*, 2:189–196, 1984.

[3] M.A. Herrada and V. Shtern. Control of vortex breakdown by temperature gradients. *Phys. Fluids*, 15:3468–3477, 2003.

[4] H.S. Husain, V Shtern, and F. Hussain. Control of vortex breakdown by addition of near-axis swirl. *Phys. Fluids*, 15:271–279, 2003.

[5] J.M. Lopez. Axisymmetrical vortex breakdown. part 1. confined swirling flow. *J. Fluid Mech.*, 221:533–552, 1990.

[6] L. Mununga, K. Hourigan, M.C. Thompson, and T. Leweke. Confined flow vortex breakdown control using a small rotating disk. *Phys. Fluid*, 16:4750–4753, 2004.

[7] J.N. Sorensen and E.A. Christensen. Direct numerical simulation of rotating fluid-flow in a closed cylinder. *Phys. Fluids*, 7:764–778, 1995.

[8] A. Spohn, M. Mory, and E.J. Hopfinger. Experiments on vortex breakdown in a confined flow generated by rotating disk. *J. Fluid Mech.*, 370:73–99, 1998.

[9] M.C. Thompson and K. Hourigan. The sensitivity of steady vortex breakdown bubbles in confined cylinder flows to rotating lid misalignment. *Journal of Fluid Mechanics*, 496:129–138, 2003.

[10] M.C. Thompson, K. Hourigan, and J. Sheridan. Three-dimensional instabilities in the wake of a circular cylinder. *Experimental Thermal and Fluid Science*, 12:190–196, 1996.

[11] H.U. Vogel. Experimentelle ergebnisse über die laminare strömung in einem zylindrischen gehäuse mit darin rotierender scheibe. *Bericht 6, Max–Planck-Institut für Strömungdforschung, Göttingen*, 1968.